Stem Cell Research & Therapy

RESEARCH

Open Access

In vitro electrophysiological drug testing on neuronal networks derived from human induced pluripotent stem cells

Giulia Parodi[1*], Giorgia Zanini[1], Linda Collo[1], Roberta Impollonia[1], Chiara Cervetto[2,3], Monica Frega[4], Michela Chiappalone[1,3] and Sergio Martinoia[1,3*]

Abstract

Background In vitro models for drug testing constitute a valuable and simplified in-vivo-like assay to better comprehend the biological drugs effect. In particular, the combination of neuronal cultures with Micro-Electrode Arrays (MEAs) constitutes a reliable system to investigate the effect of drugs aimed at manipulating the neural activity and causing controlled changes in the electrophysiology. While chemical modulation in rodents' models has been extensively studied in the literature, electrophysiological variations caused by chemical modulation on neuronal networks derived from human induced pluripotent stem cells (hiPSCs) still lack a thorough characterization.

Methods In this work, we created three different configurations of hiPSCs-derived neuronal networks composed of fully glutamatergic neurons (100E), 75% of glutamatergic and 25% of GABAergic neurons (75E25I) and fully GABAergic neurons (100I). We focused on the effects caused by antagonists of three of the most relevant ionotropic receptors of the human brain, i.e., 2-amino-5-phosphonovaleric (APV, NMDA receptors antagonist), 6-cyano-7-nitroquinoxaline-2,3-dione (CNQX, AMPA receptors antagonist), and bicuculline, picrotoxin and pentylenetetrazole (BIC, PTX, and PTZ, respectively, $GABA_A$ receptors antagonists).

Results We found that APV and CNQX completely abolished the network bursting activity and caused major changes in the functional connectivity. On the other hand, the effect of BIC, PTX and PTZ mostly affected configurations in which the inhibitory component was present by increasing the firing and network bursting activity as well as the functional connectivity.

Conclusions Our work revealed that hiPSCs-derived neuronal networks are very sensitive to pharmacological manipulation of the excitatory ionotropic glutamatergic and inhibitory ionotropic GABAergic transmission, representing a preliminary and necessary step forward in the field of drug testing that can rely on pathological networks of human origin.

Keywords Human induced pluripotent stem cells, Micro-Electrode Arrays, Electrophysiology, Drug testing

*Correspondence:
Giulia Parodi
giulia.parodi@edu.unige.it
Sergio Martinoia
sergio.martinoia@unige.it
Full list of author information is available at the end of the article

Introduction

In vitro models for drug testing provide early information and represent a valid simplified in-vivo-like assay to better comprehend the molecular pharmacology of promising compounds in the early stages of preclinical development. In particular, combining neuronal cultures with Micro-Electrode Arrays (MEAs) offers a model for electrophysiological drug screening, allowing real-time monitoring of drug diffusion and effects within the cultures. Extensively utilized in vitro models for drug testing included dissociated cultures [9, 36], whose application field is widely versatile, allowing for investigating various scenarios such as neurodevelopmental diseases [7] or physiological properties [4]. While in the literature the chemical modulation targeting rodents-derived models has been broadly explored (e.g., [9], [33]), electrophysiological variations caused by chemical modulation on neuronal networks derived from induced pluripotent stem cells (hiPSCs) have been investigated in a limited number of studies [14, 23, 35]. Nevertheless, hiPSCs-derived systems constitute a valid model to explore the electrophysiological activity of in vitro neuronal networks [26], as such cultures preserve the same phenotype of the patients [19] and better mimic the in-vivo like assay [15]. Hence, it remains an open challenge to understand whether and how different drugs are able to modulate the activity of the hiPSCs-derived in vitro networks, causing controlled electrophysiological changes. In particular, considering three of the most relevant ionotropic receptors of the human brain, i.e., NMDA, AMPA and $GABA_A$ receptors [2], the chemical modulation performed by administrating antagonists of such receptors offers the opportunity to modulate the excitatory or inhibitory contribution in a targeted manner.

In the literature, few works have explored the effect of these antagonists on hiPSCs-derived neuronal networks. Specifically, studies were mainly focused exclusively on the spiking activity [14], not investigating more complex dynamics such as the network bursting activity or functional connectivity variations, or exploited other techniques such as calcium oscillations [35]. Alternatively, research efforts focusing on the study of MEA-recorded neuronal activity, and, particularly, investigating firing and bursting patterns, targeted neuronal networks lacking a clearly defined E/I balance [23]. Nevertheless, this kind of investigation could give precious insights on the drug effects. For this reason, in this work, we created three different configurations of neuronal networks derived from hiPSCs. In particular, the three types of networks were composed of (i) fully glutamatergic neurons (100E), (ii) fully GABAergic neurons (100I), and (iii) 75% of glutamatergic and 25% of GABAergic neurons (75E25I), which faithfully mimic the in vivo environment from the E/I balance point of view [28]. We tested our model by administrating five drugs and we evaluated the changes in the activity, aiming at shedding light on the effectiveness of such drugs on the hiPSCs-derived neuronal networks. In particular, we focused on the effects caused by three drugs acting as competitive antagonists of three of the most relevant ionotropic receptors of the human brain, i.e., 2-amino-5-phosphonovaleric (APV), acting as NMDA receptors antagonist, 6-cyano-7-nitroquinoxaline-2,3-dione (CNQX), functioning as AMPA receptors antagonist, and bicuculline (BIC), working as $GABA_A$ receptors antagonist. Moreover, we tested two further drugs, which are picrotoxin (PTX, non-competitive) and pentylenetetrazole (PTZ, competitive), both acting as antagonists of $GABA_A$ receptors, but in distinct domains [13]. PTX and PTZ are central nervous system convulsant, mostly exploited to develop appropriate seizure models, by eliciting seizure activity [5, 6, 12, 27, 31]. Due to this reason and the absence of literature focused on testing these crucial drugs on in vitro hiPSCs-derived neuronal networks, we evaluated these two additional drugs. The five drugs were administered at Days In Vitro (DIV) 70: the choice of this time step was related to the network maturity [24] and beyond the GABA shift, known to occur approximately after 42–49 days [21]. We observed variations both in the dynamics—from firing to network bursting activity—and in the functional connectivity of the networks.

In conclusion, our work constitutes a significant advancement in understanding the electrophysiological changes in network dynamics and functional connectivity induced by ionotropic receptor antagonists in hiPSCs-derived cultures. This study demonstrates that hiPSCs-derived neuronal networks coupled to MEAs are highly sensitive to pharmacological manipulation of both ionotropic glutamatergic and GABAergic receptors. Consequently, it marks a substantial step forward in the field of in-vitro hiPSCs-derived models, offering a valuable innovation for testing and evaluating drugs on human neuronal pathological networks.

Methods

HiPSCs cultures maintenance

We received both Ngn2-positive and Ascl1-positive hiPSCs lines in frozen vials, kindly provided by Prof. Nadif Kasri (Radboud University Medical Centre, the Netherlands). In particular, the two hiPSCs lines (Ngn2-positive and Ascl1-positive) genetically modified and previously characterized [21] (were used to get populations of excitatory and inhibitory neurons (Fig. 1a). In particular, the excitatory neurons were obtained through the forced expression of the transcription factors Neurogenin-2 (Ngn2), while inhibitory neurons were derived through

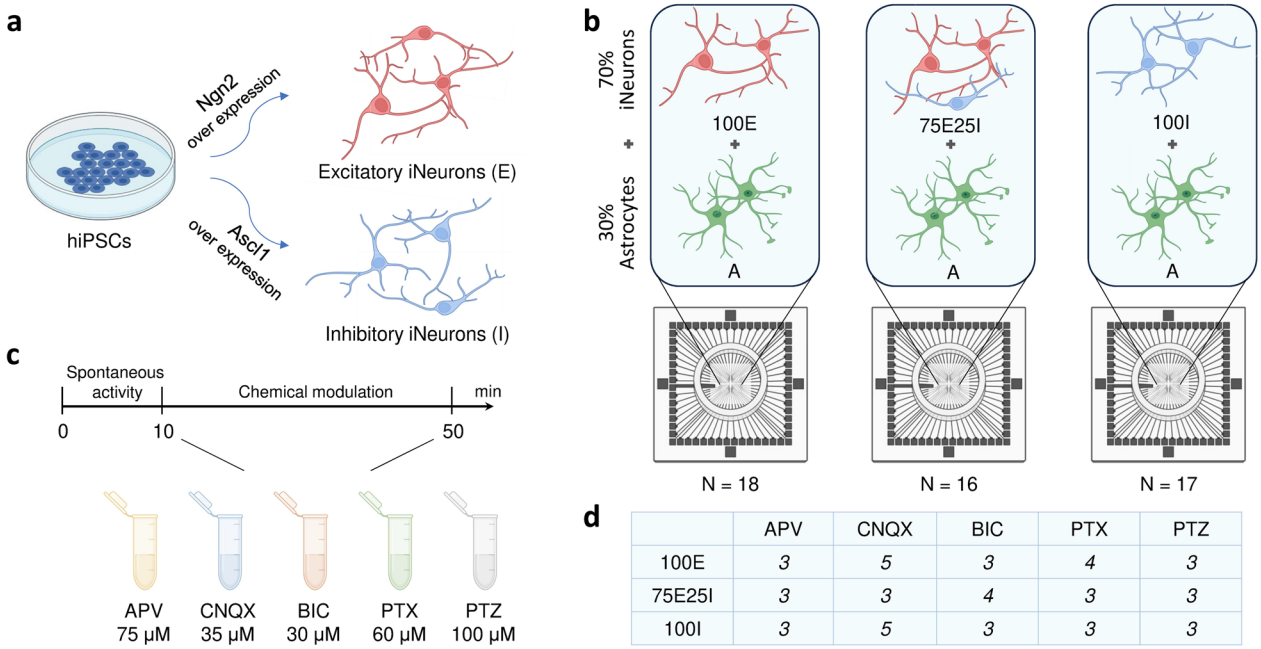

d

	APV	CNQX	BIC	PTX	PTZ
100E	*3*	*5*	*3*	*4*	*3*
75E25I	*3*	*3*	*4*	*3*	*3*
100I	*3*	*5*	*3*	*3*	*3*

Fig. 1 Experimental protocol. **a** Schematic representation of the cell culture protocol. Starting from hiPSCs cultures, excitatory (E, red) and inhibitory (I, blue) iNeurons were obtained. **b** Sketch of the three configurations obtained by varying the ratio between glutamatergic (red) and GABAergic (blue) neurons in the neuronal cultures. Neurons were co-plated with rat astrocytes (green) in the active area of the MEAs, characterized by 60 electrodes. **c** Sketch of the experimental protocol performed. The spontaneous activity was recorded for 10 min. Subsequently, one of the five drugs (i.e., APV, CNQX, BIC, PTX, or PTZ) was added to the neuronal culture medium and the electrophysiological activity was recorded for 40 min. **d** Table representing the number of the recorded neuronal cultures for each configuration and for each drug

Achaete-scute homolog 1 (Ascl1) overexpression [21]. Both lines were generated from reprogrammed fibroblasts. In particular, glutamatergic neurons were derived from healthy 30-years-old female fibroblasts (Coriell Institute for medical research, GM25256), while GABAergic neurons were derived from healthy 51-years-old male fibroblasts (KULSTEM iPSC core facility Leuven, Belgium, KSF-16-025). The lines of hiPSCs were thawed and maintained in E8 Flex medium (Thermo Fisher Scientific) supplemented with E8 supplements (2%, Thermo Fisher Scientific), penicillin/streptomycin (1%, Sigma-Aldrich), G418 (50 µg/ml, Sigma-Aldrich) and puromycin (0.5 µg/ml, Sigma-Aldrich). Excitatory cortical Layer 2/3 neurons were obtained from C1 by overexpressing mouse neural determinant Ngn2 upon doxycycline (4 µg/ml, Sigma-Aldrich) administration [10]. Inhibitory neurons were obtained from C2 by overexpressing mouse neural determinant Ascl1 (Addgene 97329) upon doxycycline (4 µg/ml, Sigma-Aldrich) and forskolin (10 µM, Sigma Aldrich) administration [21]. The hiPSCs differentiated in neurons after about 3 weeks of doxycycline and forskolin treatment [10, 30]. The cultures were preserved at stable condition (37°C, 5.5% CO_2, 95% humidity atmosphere) in the incubator. The 50% of the culture medium was refreshed every two days.

Neuronal networks generation and maintenance

The neuronal cultures were handled with the adapted pipeline presented in [34]. Briefly, we exploited polydimethylsiloxane (PDMS) rings to confine and protect the cells without creating patterned networks and affecting the neurons' viability [16, 20]. The rings were characterized by a diameter of 6 mm and height of about 1 mm and were obtained utilizing a mixture of PDMS base (Sylgard 184) and curing agent at a 10:1 (w/w) ratio, which was polymerized in oven (80 °C for 15 min). The day before the neuronal cultures plating, the rings were placed and let adhere to the Micro-Electrode Arrays (60-electrodes MEAs, Multi Channel Systems—MCS, Reutlingen, Germany) surface. The devices were sterilized in oven (120 °C for 3 h) and pre-coated overnight with poly-L-ornithine (50 µg/ml, Sigma-Aldrich) and human laminin (20 µg/ml, BioLamina). At DIV 0, glutamatergic and GABAergic neurons were detached with Accutase (Sigma-Aldrich) and mixed in the correct proportions to create our three configurations (Fig. 1b). The neurons were co-plated on the pre-treated devices with rat astrocytes (Fig. 1b) to favour the growth and the maturation of the neurons [32]. The cells were plated at a final density of 1200 cells/mm^2. Neurobasal medium (Thermo Fisher Scientific) was used to maintain the neuronal cultures. From DIV 0 to

DIV 7, the medium was enriched with B27 supplements (2%, Thermo Fisher Scientific), penicillin/streptomycin (1%, Sigma-Aldrich), GlutaMax 100X (1%, Thermo Fisher Scientific), human Brain-Derived Neurotrophic Factor (10 ng/ml, BDNF, Sigma-Aldrich), human Neurotrophin-3 (10 ng/ml, NT3, Sigma-Aldrich), doxycycline (4 µg/ml, Sigma-Aldrich) and forskolin (4 µg/ml, Sigma-Aldrich). From DIV 7 onwards, Fetal Bovine Serum (2%, Thermo Fisher Scientific) was added to the medium. From DIV 14 onwards, doxycycline and forskolin were removed from the supplemented Neurobasal medium. Half-medium change was performed every two days. The neuronal cultures plated on MEAs were stably maintained in the incubator up to DIV 70, day in which we performed the drug delivery test.

Dataset and recordings

The dataset collected for this study is composed of a total of 51 neuronal cultures over MEAs, organized in the following way: 18 100E, 16 75E25I and 17 100I. The recordings of the electrophysiological activity of such networks were performed with the MEA2100 recording system (MCS) at DIV 70, after the GABA switch. After a 10-min period of accommodation, we recorded the neuronal activity at a sampling frequency of 10 kHz in stable environmental conditions (37°C, 5% CO_2). The protocol consisted in 10-min recordings of the spontaneous electrophysiological activity, followed by 40-min recordings in presence of the chemical (Fig. 1c). The latter was performed by adding the drugs directly into the medium culture within the recording set-up. We utilized D-2-Amino-5-phosphonopentanoic acid (D-APV, 75 µM, [4]) as NMDA receptor antagonist, 6-cyano-7-nitroquinoxaline-2,3-dione (CNQX, 35 µM, [4]) as AMPA receptor antagonist, and Bicuculline (BIC, 30 µM, [36]), picrotoxin (PTX, 60 µM), and pentylenetetrazole (PTZ, 100 µM), as antagonists of $GABA_A$ receptors (Fig. 1c). The final dataset is reported in Fig. 1d.

Data analysis

The data analysis was performed exploiting in-house code implemented in MATLAB (The MathWorks, Natick, MA, USA) and SpyCode [3]. In the following subsections, we thoroughly describe the analyses carried out on the electrophysiological data.

Spiking, bursting, and network bursting activity

The data obtained from the electrophysiological recordings described above were analysed by performing the Precision Time Spike Detection [17], setting a threshold equal to 10 times the noise baseline. In addition, we set the parameters of Peak Lifetime Period and Refractory Period, required by the algorithm, both equal to 2 ms. Channels with a Mean Firing Rate (MFR, i.e., the number of spikes over the whole recording time) lower than 0.1 spikes/s (spk/s) have been removed from the analysis, since they were considered inactive [21, 22]. Subsequently, the burst detection was carried out based on the distribution of logarithmic ISI [25] and evaluating bursts composed of at least 5 spikes. Electrodes with a Mean Bursting Rate (MBR) lower than 0.4 bursts/min were discarded [21, 22]. Neuronal networks with an amount of bursting electrodes lower than 10% were not considered for further analysis related to the bursting and network bursting activity. The network burst detection was performed based on the burst trains and an event was defined as a network burst if the number of the involved electrodes was more than 25% of bursting electrodes. Concerning the analysis of the chemically modulated neuronal networks, we divided the 40-min recordings into 5-min-long bins in order to analyse with greater resolution the behaviour over time of the neuronal networks. In particular, we computed the Instantaneous Firing Rate (IFR, i.e., the spiking frequency in each bin), the Network Bursting Rate (NBR), and the number of network bursting units as the number of channels involved in the network burst events. Finally, we considered the first 20 min out of the total 40 min, and we repeated the analysis of the IFR with 1-min-long bins, in order to observe the effect of the drugs in more detail. All the values presented in this study were normalized with respect to the spontaneous activity of each group of neuronal networks treated with the same drug.

Cross-correlation based analysis

Concerning the cross-correlation based analysis, we considered the timing at which a channel fires (target channel β), evaluating a relationship with the firing of another spikes train (reference channel α), [29]. Hence, identified a reference channel α and a target channel β, the correlation function $C_{\alpha\beta}(\tau)$ denoted the probability of observing at the time $(t+\tau)$ a spike in the target train α, given a spike in the reference train β at the time t. We computed the cross-correlograms considering the correlation function in a window of ± 150 ms with a binning equal to 0.2 ms. A relevant peak in the cross-correlogram delineated a functional connection, whose amplitude can be related to the levels of synchronization between the neuronal spike trains. To this end, we computed the maximum value normalized between [0, 1] of each pairwise cross-correlogram (i.e., C_{peak}). From the unthresholded connectivity matrix, we computed the number of links (i.e., the number of connections between all the electrodes) and the number of nodes (i.e., the number of electrodes that have at least one link) to quantify the variation of the network-developed functional connections

after the addition of the drugs in the culture medium. Finally, we assessed the C_{peak} of the strongest 200 connections [11] to evaluate the variation in their strength after the drug treatment.

Statistical analysis

The statistical analyses were performed in MATLAB (The MathWorks, Natick, MA, USA). The distribution of the data was evaluated by exploiting the Kolmogorov–Smirnov normality test. As the data were not normally distributed, the statistical analyses were computed with the non-parametric Kruskal–Wallis test. To determine statistical differences, p-values < 0.05 were considered significant. In the text, the values are reported as mean ± standard error of the mean, unless differently stated. In the scatter plots, asterisks over the dots represent a statistical difference with respect to the spontaneous activity.

Results

Blocking NMDA, AMPA and $GABA_A$ receptors affected the firing patterns

To understand the effect of the drugs on the electrophysiological activity of the neuronal networks, we first considered the single-channel-level dynamics by analysing the normalized IFR during the spontaneous and chemically evoked activity. The 100E configuration—although not significant with respect to the spontaneous (i.e. not treated) initial condition—showed a slow decrease of the IFR trend when exposed to APV (Fig. 2a, Table S1, S2), while CNQX led to a rapid decrease of the 100E firing, noticeable within the first 5 min after that the drugs were added to the medium (Fig. 2d, Table S1, S2). On the other hand, BIC—as expected—maintained the firing pattern of this configuration constant (Fig. 2g, Tables S1, S2). Concerning the 75E25I configuration, a similar trend can be observed with respect to the 100E, when APV (Fig. 2b) and CNQX (Fig. 2e) were added to the medium: both drugs caused a decrease of the IFR

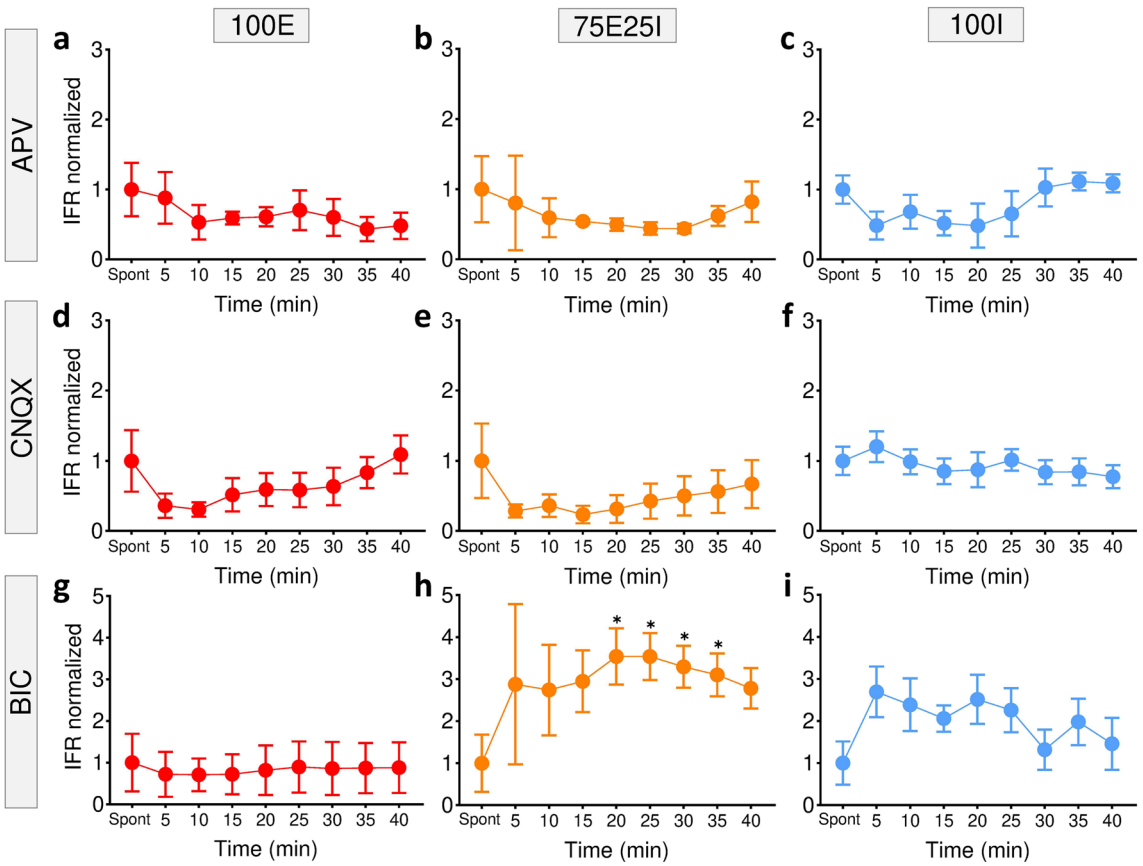

Fig. 2 Spiking activity characterization during the chemical modulation. **a**–**i** Normalized Instantaneous Firing Rate (IFR) of 100E (red), 75E25I (orange), and 100I (blue) configurations when APV (first row), CNQX (second row), or BIC (third row) were used. The timepoint "Spont" represents the normalized firing rate computed over the 10-min recording of the spontaneous activity. Data are represented with the mean (dot) and the standard error of the mean (whiskers) (∗ refers to $p < 0.05$)

with a faster timing when CNQX was used (Tables S1, S2). BIC, instead, resulted in an increased firing activity of the 75E25I (Fig. 2h, Tables S1, S2), noticeable from the first 5 min after the presence of the drug. Lastly, the 100I configuration, in the case of APV treatment (Fig. 2c, Tables S1, S2), showed a decrease—not statistically significant—in the IFR during the first 25 min, stabilizing again close to the values of the spontaneous activity after about 30 min, while exhibited an increase when treated with BIC, showing a similar timing of action with respect to the 75E25I configuration when treated with the same drug.

Since the major changes in the firing patterns mostly occurred within the first 20 min after the drug delivery, we focused the analysis of the IFR in this range with a smaller bin size, i.e., 1 min (Fig. S1). The trends of the 1-min-binned IFR for each configuration and each drug showed a higher variability during the first 5–10 min due to the possible perturbation of the drug injection within the neuronal networks [9]. After this interval, the effect of the drugs on the IFR stabilized. For this reason, we chose to analyse more thoroughly the differences between the spontaneous and the chemically evoked activity between 10 to 15 min after the drug addition (see Sect. "Short-term effects of drug treatment"). Finally, concerning the bursting pattern, the 100I configuration exhibited a number of bursting units under the threshold for all the cultures (Fig. S2a)—as expected—since these neuronal networks were characterized by a tonic firing pattern (Fig. S3a) and uncorrelated activity (Fig. S3b). For this reason, the neuronal networks composed of exclusively GABAergic neurons (i.e., 100I) were excluded from further analysis related to network bursting events and functional connectivity investigations.

APV and CNQX abolished the network events

To understand the effect of the drugs on the network-level activity, we initially evaluated the electrophysiological activity from a qualitative point of view by observing the raster plots and the cumulative instantaneous firing rate profiles (Fig. 3a). Both configurations, i.e., 100E and 75E25I, showed sustained spontaneous activity characterized by repeated bursting and network bursting events (Fig. 3a). In the presence of APV or CNQX, the network bursting events were completely abolished in both configurations resulting in solely random activity (Fig. 3a). On the other hand, BIC appeared to slightly decrease the rate of network events in the 100E, while it increased the frequency of network bursts in the 75E25I. Quantifying the NBR, it revealed that both APV and CNQX drastically reduced the NBR in the 100E (Fig. 3b, c, Table S3, S4) and 75E25I (Fig. 3e, f, Table S3, S4) configurations. It is worth to highlight that both drugs affected the rate of the network bursting events of the physiological configuration (i.e., 75E25I) since the first 5 min after that the drugs were added to the medium, while the effects on the fully excitatory networks were appreciable after 10 and 5 min from the APV and CNQX presence, respectively. Finally, BIC halved the frequency of network events of the 100E networks (Fig. 3d, Table S3, S4), while, conversely, caused a significant increase in the network bursting rate of the 75E25I configuration (Fig. 3g, Table S3, S4).

Short-term effects of drug treatment

To better analyse the impact of the drugs on network bursting patterns, we compared the spontaneous activity with the chemically evoked activity between 10 and 15 min after drug treatment (see Sect. "Blocking NMDA, AMPA and GABAA receptors affected the firing patterns"). Major changes were exhibited by the network bursting activity, in which both APV and CNQX induced a reduction of the network bursting units (Fig. 4a, Tables S5, S6) in both 100E and 75E25I, but significant only for the 100E. On the other hand, BIC induced the generation of network events characterized by a comparable number of units for both 100E and 75E25I (Table S5, S6). The NBR resulted to be highly affected by the drugs (Fig. 4b). In particular, both APV and CNQX caused a strong, statistical decrease with respect to the spontaneous activity in the NBR of both 100E ($p_{APV}=0.0463$, $p_{CNQX}=0.0150$) and 75E25I ($p_{APV}=0.0463$) configurations, leading to values close to zero ($NBR_{100E\_APV}=0.06\pm0.03$, $NBR_{75E25I\_APV}=0.01\pm0.01$, $NBR_{100E\_CNQX}=0.13\pm0.10$, $NBR_{75E25I\_CNQX}=0.09\pm0.08$) proving the abolishment of the network bursting activity, as hinted by the raster plots of Fig. 3a. Conversely, BIC led to a statistical increase in the rate of the network events in the 75E25I ($NBR_{75E25I\_BIC}=3.09\pm0.40$), and a slight—but statistical—decrease in the 100E configuration ($NBR_{100E\_BIC}=0.44\pm0.15$), as qualitatively suggested by the raster plots in Fig. 3a. Since APV and CNQX completely suppressed the network events of the cultures, we then investigated changes in the average network burst shapes and in the network burst duration (NBD) in the neuronal networks treated with BIC (Fig. 4c, d, Table S7). The network burst shape showed an increased amplitude, both in 100E and 75E25I when treated with BIC. Moreover, an increase in the network burst duration can be observed in both configurations ($NBD_{100E\_BIC}=1.90\pm0.49$, $NBD_{75E25I\_BIC}=1.48\pm0.20$), albeit not statistical.

Drug-driven changes in the functional connectivity

The neuronal connectivity showed to be affected by the drug treatments as well as the neuronal dynamics. Specifically, the use of APV resulted in a drastic reduction in the strength of the connections in both the 100E

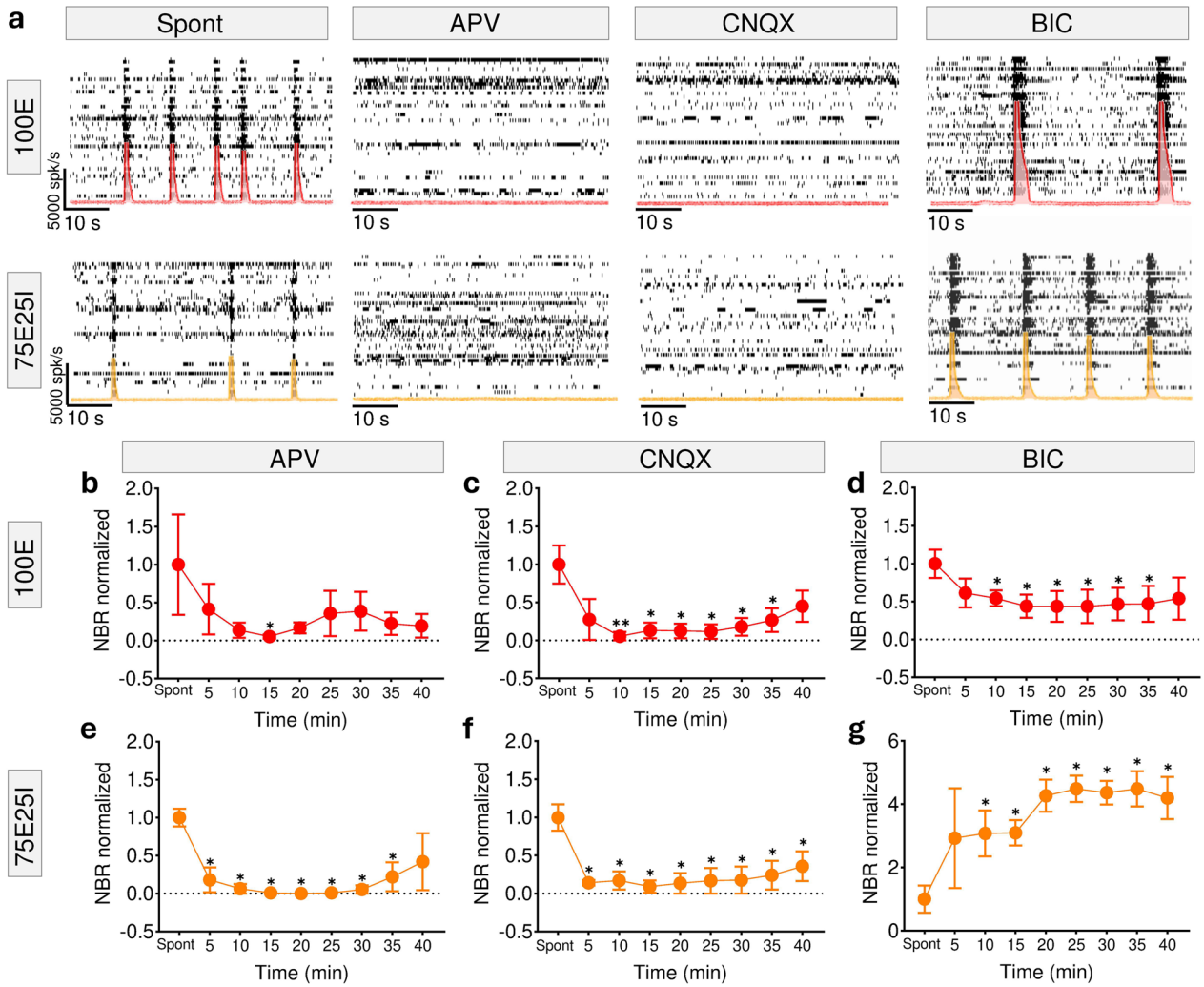

Fig. 3 **a** Representative raster plots and respective cumulative instantaneous firing rate profiles (bin = 10 ms, overlapped) of the electrophysiological activity of the 100E (red) and 75E25I (orange) configurations in spontaneous conditions (first column) and after APV (second column), CNQX (third column), and BIC (fourth column) administration. A black dot represents a detected spike, while a dense black band indicates a network burst event. **b-g** Network bursting activity characterization during the chemical modulation. Normalized Network Bursting Rate (NBR) of 100E (red) and 75E25I (orange) configurations when APV (**b**, **e**), CNQX (**c**, **f**), or BIC (**d**, **g**) were used. The timepoint "Spont" represents the normalized NBR computed over the 10-min recording of the spontaneous activity. Data are represented with the mean (dot) and the standard error of the mean (whiskers) (∗ refers to $p < 0.05$ and ∗ ∗ to $p < 0.01$)

and 75E25I configurations, as shown in the connectivity maps and graphs (Fig. 5). On the other hand, it was difficult to evaluate qualitative changes in the number of links and the number of nodes from such intricate structures, although a reduction of both features was suggested. For what concerns CNQX, the AMPA receptor antagonist caused a reduction of the connection strength and the number of links and nodes as well as in the case of APV usage in both 100E and 75E25I (Fig. 5). Finally, BIC did not induce observable changes in the connectivity of the 100E configuration, while a substantial increase in the strength and in the number of links can be observed in the connectivity map and graph of the 75E25I configuration (Fig. 5). As a step forward, we computed the number of nodes and links during the chemical stimulated activity, by distinguishing the new ones, those which remained stable those which disappeared when treated with the drugs (Fig. 6). APV led to a reduction of both nodes and links, especially in the 100E configuration (Fig. 6a, d), as well as CNQX, in which a high number of extinguished nodes and links can be observed (Fig. 6b, e). On the other hand, BIC usage confirms to not affect particularly the 100E configuration (Fig. 6c), while in

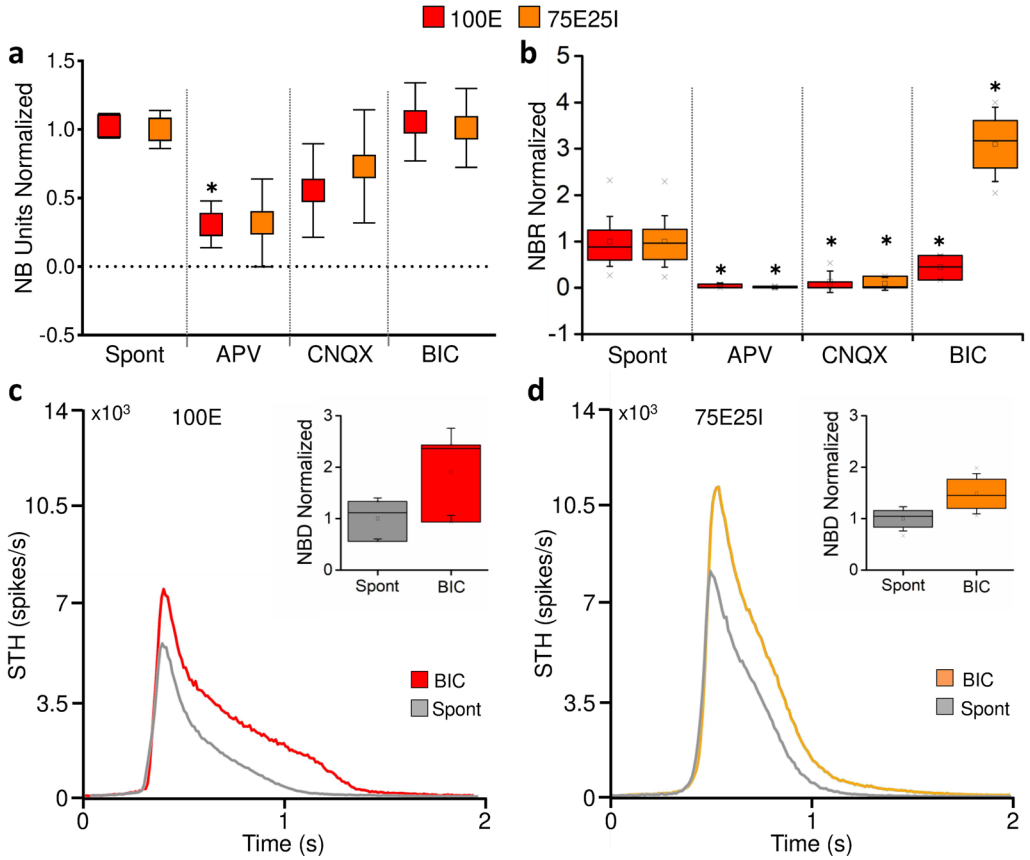

Fig. 4 Drugs' effect in the 10–15 min after the administration. **a** Plot of the normalized number of network bursting (NB) units for 100E (red) and 75E25I (orange) configurations. **b** Box plots of the normalized Network Bursting Rate (NBR) for each configuration. **c**, **d** Average network burst shapes (Spike Time Histogram, STH) for the spontaneous (grey) and the BIC-modulated activity for the 100E (**c**, red) and 75E25I (**d**, orange) configurations. Inset: box plots of the Network Burst Duration (NBD) for each configuration in spontaneous (grey) and BIC modulated (red or orange) conditions. Scatter plots are represented with the mean (dot) and the standard error of the mean (whiskers). Box plots are represented with the percentile 25–75 (box), the standard deviation (whiskers), the median (line), the mean (square), and the minimum and maximum (crosses) values (∗ refers to $p < 0.05$)

the 75E25I configuration led to a noticeable increase in both the number of new nodes (28%) and the number of new links (70%) (Fig. 6f). Finally, we evaluated the C_{peak} values (Table S8), indicating the strength of the connections. The APV usage showed a decrease in the C_{peak} values in both 100E and 75E25I configurations (Fig. 6g, h, $C_{peak\_100E\_spont} = 0.23 \pm 0.03$, $C_{peak\_100E\_APV} = 0.05 \pm 0.03$, $C_{peak\_75E25I\_spont} = 0.22 \pm 0.06$, $C_{peak\_75E25I\_APV} = 0.13 \pm 0.06$), although statistically significant only in the case of 100E ($p_{APV} = 0.018$). On the other hand, CNQX showed a slight decrease in the C_{peak} value exclusively for the 75E25I configuration (Fig. 6h, $C_{peak\_75E25I\_CNQX} = 0.13 \pm 0.06$). Lastly, BIC did not cause any changes in the strength of the connections of the 100E (Fig. 6g), leading to an increase of such value only in the heterogeneous configuration (Fig. 6h, $C_{peak\_75E25I\_BIC} = 0.37 \pm 0.08$).

The presence of PTX and PTZ showed comparable effects with respect to BIC treatment

To conclude our work, we investigated the effects of two further drugs, i.e., PTX and PTZ, antagonist of $GABA_A$ receptors. Retracing the main steps highlighted for APV, CNQX, and BIC, we first evaluated the IFR of the neuronal networks after the drug treatment. PTX did not affect the firing pattern of the 100E configuration (Fig. 7a, Table S9, S10), while PTZ caused a slight decrease during the first 10 min, rapidly restored after 15 min (Fig. 7d, Table S9, S10). For what concern the effect of PTX and PTZ on the 75E25I configuration, the presence of such drugs showed similar effect with respect to BIC usage, that is an increase of the IFR (Fig. 7b, e, Table S9, S10). Nevertheless, a different time of action of the drugs can be observed: while BIC effect was quite instantaneous (noticeable within the first 5 min), PTX and PTZ showed a slower increase of the IFR, appreciable after

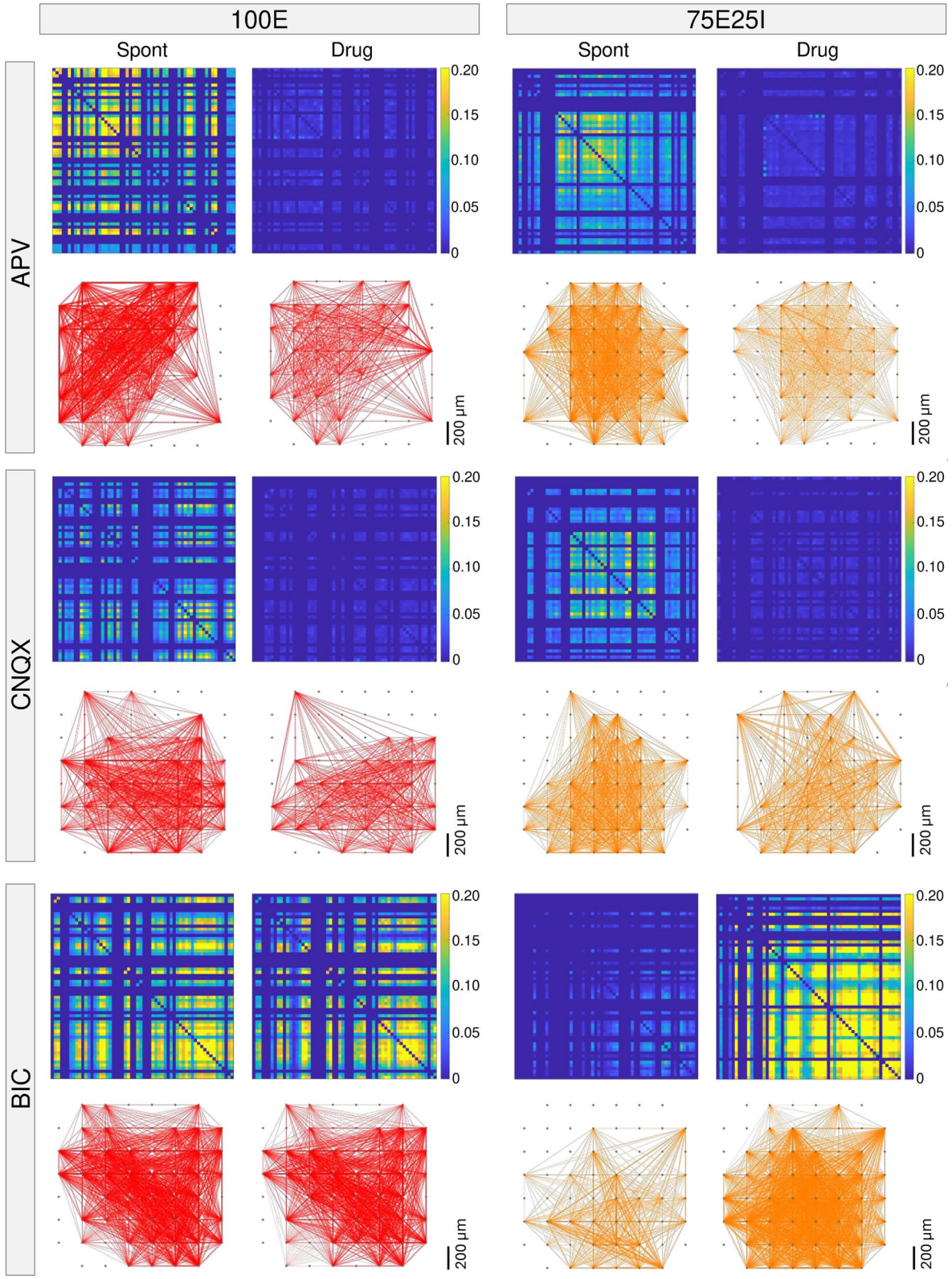

Fig. 5 Functional connectivity maps and graphs. Representative connectivity maps and connectivity graphs of 100E (red) and 75E25I (orange) configurations. In each pair, the functional connectivity map/graph of the spontaneous activity (on the left) is compared with the one after the drug treatment (on the right). In the connectivity maps, the connection between two units is represented by a pixel which colour represents its strength. In the connectivity graphs, each node is represented by dots and functional connections are represented with edges

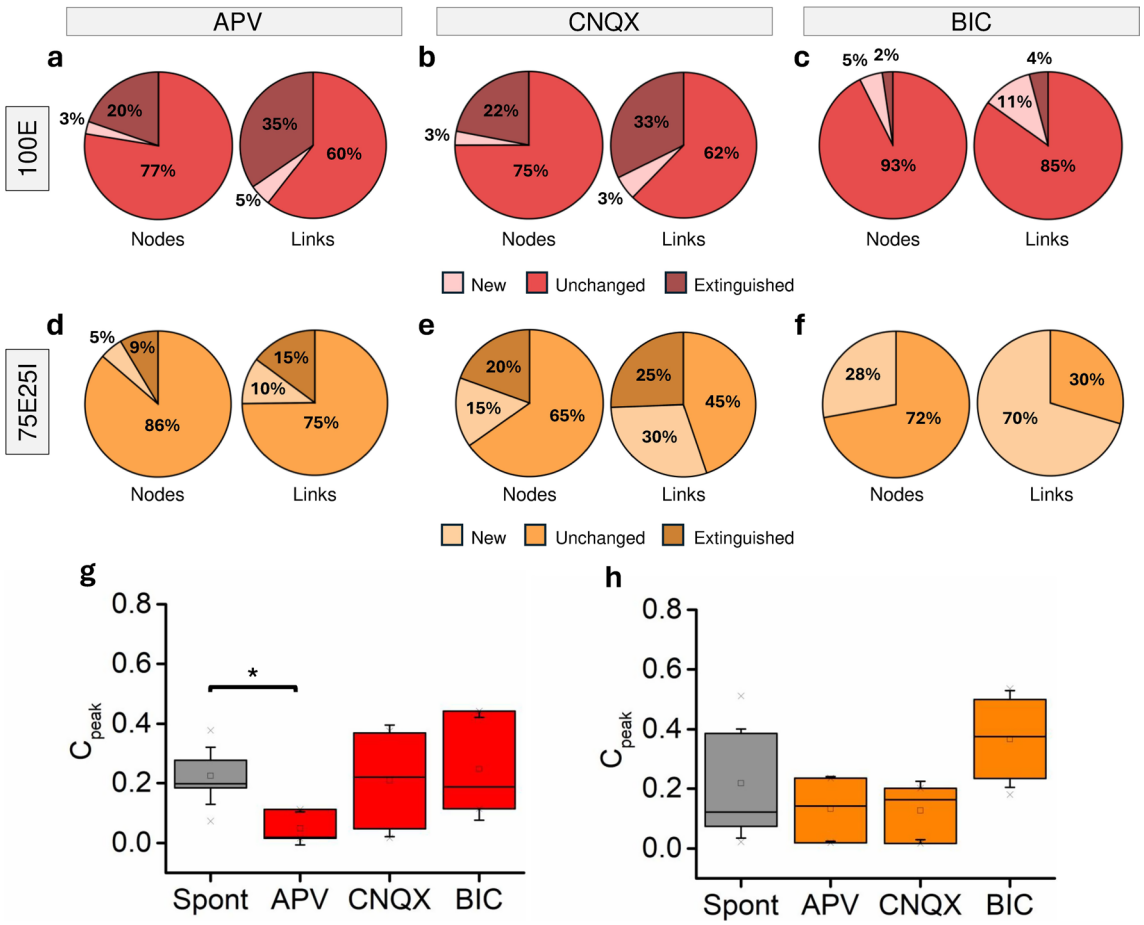

Fig. 6 Characterization of the functional connectivity. **a**–**f** Pie charts of the number of edges and number of links new, unchanged, and extinguished with respect to the spontaneous activity for each configuration and for each administrated drug. **g**–**h** Box plots of the C_{peak} values of the 100E **g** and 75E25I **h** configurations. Box plots are represented with the percentile 25–75 (box), the standard deviation (whiskers), the median (line), the mean (square), and the minimum and maximum (crosses) values (∗ refers to $p < 0.05$)

about 15/20 min after the drug treatment. Alongside, the 100I configuration was affected exclusively by the usage of PTZ, which induced an increase of the IFR (Fig. 7f, Table S9, S10), while PTX did not provoke any changes in the firing pattern (Fig. 7c, Table S9, S10). Concerning the neuronal network events, the NBR of the 100E configuration after both PTX and PTZ treatment showed a decrease as noticed for the BIC usage (Fig. 7g, j, Table S11, S12). On the other hand, the 75E25I configuration showed different trends when treated with PTX or PTZ (Table S11, S12): the first one caused an initial slight decrease of the NBR, rapidly restored within 15 min (Fig. 7h); the second one provoked a slight increase of the NBR, which continued throughout the recording time (Fig. 7k). Finally, both PTX and PTZ led to an increase of the Network Burst Duration (NBD; Fig. 7i, l; $NBD_{100E\_PTX} = 1.43 \pm 0.26$, $NBD_{75E25I\_PTX} = 2.01 \pm 0.42$, $NBD_{100E\_PTZ} = 1.83 \pm 0.56$, $NBD_{75E25I\_PTZ} = 1.31 \pm 0.30$, Table S15), although without significant differences (Table S16), in both configurations, as well as in the case of BIC.

Discussion

In this study, we proposed an innovative drug testing model in which we exploited human induced pluripotent stem cells to understand whether and how these neuronal cultures were sensitive to pharmacological manipulation. We created three different configurations, both homogeneous and heterogeneous—in terms of excitatory and inhibitory neuronal cells—to evaluate the effect of the individual drugs either on excitatory or inhibitory populations, and on cultures with a physiological E/I balance.

We performed the recordings and the chemical modulation at DIV 70, when the networks were mature [24] and characterized by a hyperpolarizing effect of the GABA, as the GABA shift occurs at around DIV 42 [21]. Our results showed that APV and CNQX caused a decrease in the firing, as expected [4, 14, 23]. On the

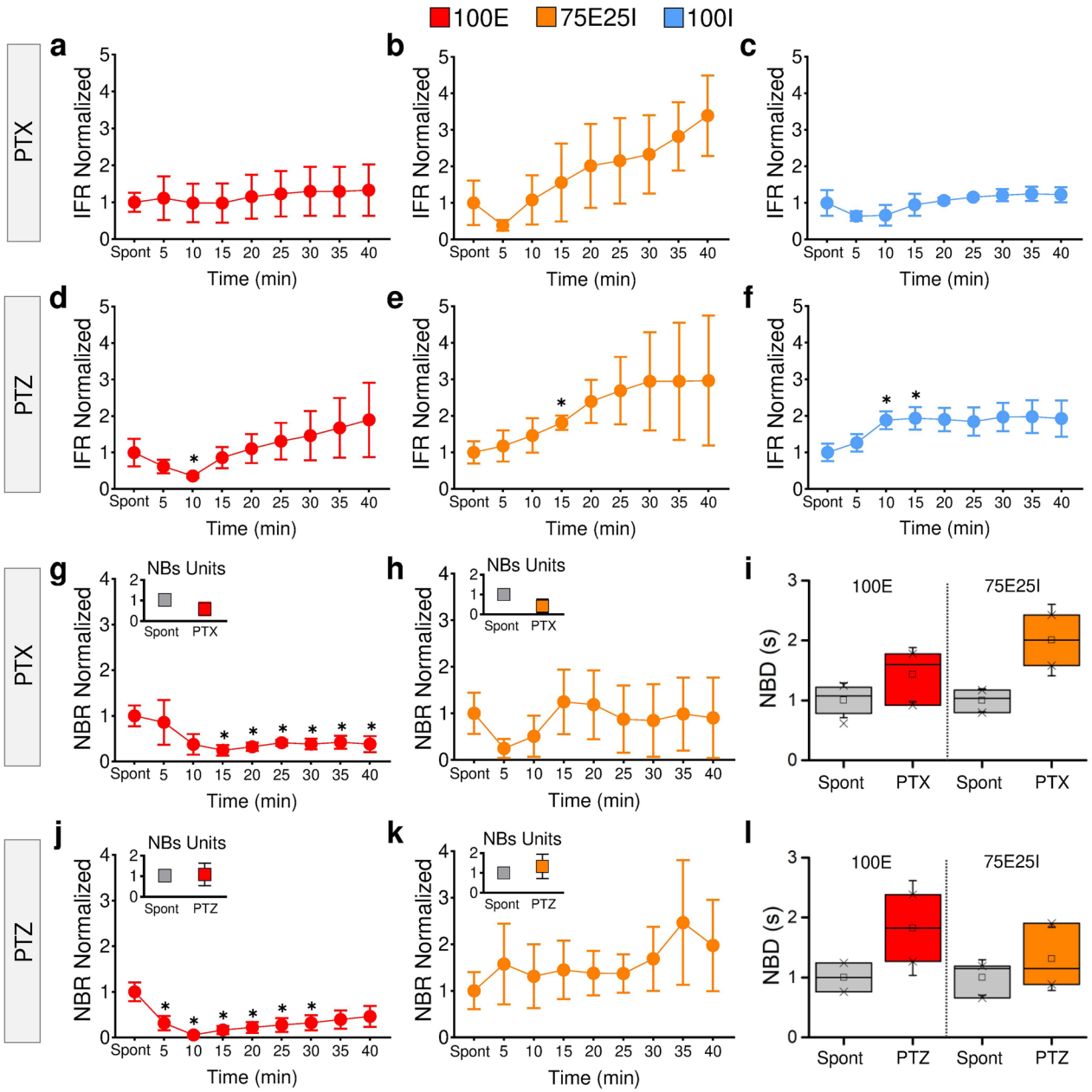

Fig. 7 Characterization of PTX e PTZ effects. **a**–**c** Normalized Instantaneous Firing Rate (IFR) over time of the 100E (red), 75E25I (orange), and 100I (blue) configurations when PTX was used. **d**–**f** Normalized IFR over time of the 100E (red), 75E25I (orange), and 100I (blue) configurations when PTZ was used. **g**–**h** Normalized Network Bursting Rate (NBR) over time of the 100E (red) and 75E25I (orange) configurations in the presence of PTX. Insets: Normalized number of network bursting units of the configurations in the spontaneous and PTX evoked conditions. **i** Normalized Network Burst Duration (NBD) of the 100E (left) and 75E25I (right) configurations in spontaneous (grey) and PTX evoked conditions (red and orange, respectively). **j**–**k** Normalized Network Bursting Rate (NBR) over time of the 100E (red) and 75E25I (orange) configurations in the presence of PTZ. Insets: Normalized number of network bursting units of the configurations in the spontaneous and PTZ evoked conditions. **l** Normalized Network Burst Duration (NBD) of the 100E (left) and 75E25I (right) configurations in spontaneous (grey) and PTZ evoked conditions (red and orange, respectively). Scatter plots are represented with the mean (dot) and the standard error of the mean (whiskers). Box plots are represented with the percentile 25–75 (box), the standard deviation (whiskers), the median (line), the mean (square), and the minimum and maximum (crosses) values (∗ refers to $p < 0.05$)

other hand, BIC increased the spiking frequency of heterogeneous and fully GABAergic networks. In addition, the network bursting activity proved to be the dynamics pattern most significantly affected by the drug treatment. Indeed, APV and CNQX severely reduced the activity of network's events leading to a network bursting rate close to zero, both in the heterogeneous and fully glutamatergic networks, in line with what was observed in the literature for rodent-based networks [4]. It is worth to notice that CNQX showed a more rapid effect on the hiPSCs-derived neuronal networks with respect to the APV. This strongest impact on the dynamics is reasonable considering that NMDA receptors require AMPA receptors to be activated [18]. Thus, in the presence of AMPA antagonist (i.e. CNQX), the resulted effects were the summation of both AMPA and—consequently—NMDA receptors blockage. At the same time, BIC led to a decrease in network activity in the 100E cultures. The effect of such a drug on purely excitatory networks is attributable to the fact that glutamatergic neurons in merely excitatory cultures still develop $GABA_A$ receptors [37] and that astrocytes, present in our networks, express abundant $GABA_A$ receptors as well [8]. It is worth to emphasize that the significance of this indirect effect may vary depending on the density of astrocytes present within the cellular culture. To deepen this aspect, it would be noteworthy to perform an assessment of the astrocytes in the final composition at DIV 70 and to evaluate the influence of different densities of astrocytes. Furthermore, the decrease in NBR observed in these cultures following the usage of BIC may be attributed to an altered homeostatic balance within the networks. It is worth noting that, since the 100E configuration does not mimic a physiological condition, the response to BIC could differ from what might be anticipated under normal circumstances. The 75E25I configuration, however, showed a clear increase in the frequency of network events, as expected [36]. As regards the effect of BIC on the duration of network bursts, it led to a notable increase of the parameter. Indeed, GABAergic neurons are the main responsible for the neuronal excitability and for synchronizing network events, acting by compressing the duration of the network bursts [1, 24]. Since BIC acted directly on the GABA receptors, it blocked inhibitory neurons causing an increase in the duration of the network events.

In our study, we took a further step by characterizing the functional connectivity of networks derived from hiPSCs in the context of drug testing, an aspect not previously explored in the literature. Our cross-correlation analysis revealed that APV and CNQX not only affected the network dynamics, but also systematically reduced the number of links and nodes in the networks, leading to a decrease in the strength of connections. On the other hand, BIC did not bring particular differences in the connectivity regarding the purely excitatory networks, while caused an increase in the links, nodes, and strength of connections in the heterogeneous networks.

Finally, we tested two additional drugs, namely PTX and PTZ, which are particularly important in the field of neuroscience being used to induce convulsant phenotypes [6, 27]. These two aforementioned drugs have been mainly used in animal-derived or in vivo models. In our human-derived system, being $GABA_A$ receptor antagonists, both PTX and PTZ showed effects comparable to BIC when added to both homogeneous excitatory and heterogeneous networks, demonstrating that hiPSCs-derived networks are sensitive to pharmacological manipulation of the inhibitory ionotropic GABAergic transmission through PTX e PTZ.

Conclusions

In summary, our work represents a new platform and a well-characterized starting point for further advances in drug testing exploiting human-derived neuronal networks. In the literature, this topic has been poorly addressed despite its importance. Indeed, the main advantage of these networks is represented by the ability to inherently carry the same phenotype as the donor, thus constituting a powerful tool in the field of personalized medicine. Moreover, electrophysiological characterization can open new scenarios and give insights to peculiarities of neuronal activity that can remain hidden with other methodologies. In the literature, few works deepened this topic by addressing basic electrophysiological characteristics, such as the firing pattern [14]. However, this may limit the sighting of differences or peculiar aspects of these networks that can be highlighted with more in-depth analysis such as functional connectivity reported here. In conclusion, our model represents an important advancement for unravelling electrophysiological changes in the network dynamics and functional connectivity caused by drugs within hiPSCs-derived cultures. It therefore represents a step forward in the field of in-vitro hiPSCs-derived models that can be a valuable tool for testing and evaluating drugs on human pathological networks.

Abbreviations

APV	D-2-Amino-5-phosphonopentanoic acid
BIC	Bicuculline
CNQX	6-Cyano-7-nitroquinoxaline-2,3-dione
DIV	Days in vitro
hiPSCs	Human induced pluripotent stem cells
IFR	Instantaneous firing rate
MEAs	Micro-electrode arrays
MBR	Mean bursting rate
MFR	Mean firing rate
NBD	Network burst duration
NBR	Network bursting rate

PTX Picrotoxin
PTZ Pentylenetetrazole
STH Spike time histogram

Supplementary Information

The online version contains supplementary material available at https://doi.org/10.1186/s13287-024-04018-2.

Supplementary file 1.

Acknowledgements
The authors wish to thank Prof. Nadif Kasri (Radboud University Medical Centre) for kindly supplying the hiPSCs cultures; Dr Mariateresa Tedesco for gently providing rat astrocytes and, together with Prof. Anna Fassio, Dr Bruno Sterlini, Dr Martina Brofiga, and Dr Martina Servetti, for their kind advice on the experimental procedure and useful discussion. The authors declare that they have not used Artificial Intelligence in this study.

Author contributions
GP: conception and design, acquisition, analysis, interpretation of data, writing—original draft. GZ: acquisition, analysis, writing—review and editing. LC: analysis, review and editing. RI: acquisition. CC: review and editing. MF: supervision, review. MC: supervision, validation, review and editing. SM: project administration and resources, supervision, validation. All authors read and approved the final manuscript.

Funding
Work supported by #NEXTGENERATIONEU (NGEU) and funded by the Ministry of University and Research (MUR), National Recovery and Resilience Plan (NRRP), Project MNESYS (PE0000006) —A Multiscale integrated approach to the study of the nervous system in health and disease (DN. 1553 11.10.2022).

Availability of data and materials
The datasets used and analysed during the current study are available from the corresponding author on reasonable request.

Declarations

Ethics approval and consent to participate
The experimental protocol was approved by the European Animal Care Legislation (2010/63/EU), by the Italian Ministry of Health in accordance with the D.L. 116/1992 and by the guidelines of the University of Genova (Prot. 75F11.N.6JI, 08/08/2018). We received the Ngn2-positive and Ascl1-positive hiPSCs lines in frozen vials, kindly provided by Prof. Nadif Kasri (Radboud University Medical Centre, the Netherlands). The genetically modified organism (GMO) approval under which the lines have been used is IG22-071. The two lines provided by our collaborators were previously characterized [21]. The lines were infected, according to a previously published protocol [10], with lentiviral constructs encoding rtTA combined with Ngn2 (Control line 1) or Ascl1 (Control line 2) to generate doxycycline-inducible excitatory or inhibitory neurons arrays [21, 22]. Both lines were generated from reprogrammed fibroblasts. Control line 1 (C1, healthy 30-years-old female, Ngn2) was reprogrammed via episomal reprogramming (Coriell Institute for medical research, GM25256). Control line 2 (C2, healthy 51-years-old male, Ascl1) was reprogrammed via a non-integrating Sendai virus (KULSTEM iPSC core facility Leuven, Belgium, KSF-16-025). Karyotypes of hiPSCs lines were verified, and hiPSCs lines were tested for pluripotency and genomic integrity based on single nucleotide polymorphism arrays [21, 22]. We declare that the research was conducted in accordance with the principles embodied in the Declaration of Helsinki and in accordance with local statutory requirements.

Consent for publication
Not applicable.

Competing interests
The authors declare that they have no competing interests.

Author details
[1]Department of Informatics, Bioengineering, Robotics, and Systems Engineering (DIBRIS), University of Genova, Genova, Italy. [2]Department of Pharmacy (DIFAR), University of Genova, Genova, Italy. [3]IRCCS Ospedale Policlinico San Martino, Genova, Italy. [4]Department of Clinical Neurophysiology, University of Twente, 7522 NB Enschede, The Netherlands.

Received: 1 July 2024 Accepted: 25 October 2024
Published online: 17 November 2024

References

1. Baltz T, de Lima AD, Voigt T. Contribution of GABAergic interneurons to the development of spontaneous activity patterns in cultured neocortical networks. Front Cell Neurosci. 2010;4:1471. https://doi.org/10.3389/fncel.2010.00015.
2. Ben-Ari Y, Khazipov R, Leinekugel X, Caillard O, Gaiarsa JL. GABAA, NMDA and AMPA receptors: a developmentally regulated `ménage à trois'. Trends Neurosci. 1997;20(11):523–9. https://doi.org/10.1016/S0166-2236(97)01147-8.
3. Bologna LL, Pasquale V, Garofalo M, Gandolfo M, Baljon PL, Maccione A, Martinoia S, Chiappalone M. Investigating neuronal activity by SPYCODE multi-channel data analyzer. Neural Netw. 2010;23(6):685–97. https://doi.org/10.1016/J.NEUNET.2010.05.002.
4. Bonzano L, Bove M, Martinoia S. Effects of NMDA and non-NMDA receptors antagonists on the dynamic behavior of cultured cortical networks. Neurocomputing. 2006;69(16–18):1897–903. https://doi.org/10.1016/j.neucom.2005.11.014.
5. Borowicz, K. K. (2009). HORMONES AND GENDER | Sex and Seizure Sensitivity. *Encyclopedia of Basic Epilepsy Research*, 519–522. https://doi.org/10.1016/B978-012373961-2.00029-1
6. Cremer CM, Palomero-Gallagher N, Bidmon HJ, Schleicher A, Speckmann EJ, Zilles K. Pentylenetetrazole-induced seizures affect binding site densities for GABA, glutamate and adenosine receptors in the rat brain. Neuroscience. 2009;163(1):490–9. https://doi.org/10.1016/j.neuroscience.2009.03.068.
7. Farkhondeh A, Li R, Gorshkov K, Chen KG, Might M, Rodems S, Lo DC, Zheng W. Induced pluripotent stem cells for neural drug discovery. Drug Discov Today. 2019;24(4):992–9. https://doi.org/10.1016/j.drudis.2019.01.007.
8. Fraser DD, Mudrick-Donnon LA, Macvicar BA. Astrocytic GABA receptors. Glia. 1994;11(2):83–93. https://doi.org/10.1002/GLIA.440110203.
9. Frega M, Pasquale V, Tedesco M, Marcoli M, Contestabile A, Nanni M, Bonzano L, Maura G, Chiappalone M. Cortical cultures coupled to microelectrode arrays: a novel approach to perform in vitro excitotoxicity testing. Neurotoxicol Teratol. 2012;34(1):116–27. https://doi.org/10.1016/j.ntt.2011.08.001.
10. Frega M, Van Gestel SHC, Linda K, Van Der Raadt J, Keller J, Van Rhijn JR, Schubert D, Albers CA, Kasri NN. Rapid neuronal differentiation of induced pluripotent stem cells for measuring network activity on microelectrode arrays. J Visual Exp. 2017;2017(119):54900. https://doi.org/10.3791/54900.
11. Garofalo M, Nieus T, Massobrio P, Martinoia S. Evaluation of the performance of information theory-based methods and cross-correlation to estimate the functional connectivity in cortical networks. PloS One. 2009;4(8):6482. https://doi.org/10.1371/JOURNAL.PONE.0006482.
12. Haberer LJ, Pollack GM. Central nervous system uptake kinetics of pentylenetetrazol in the developing rat. Biopharm Drug Dispos. 1991;12(1):59–71. https://doi.org/10.1002/BDD.2510120107.
13. Huang RQ, Bell-Horner CL, Dibas MI, Covey DF, Drewe JA, Dillon GH. Pentylenetetrazole-induced inhibition of recombinant γ-aminobutyric acid type A (GABAA) receptors: mechanism and site of action. J Pharmacol Exp Therap. 2001;298(3):986–95.
14. Kang KR, Kim CY, Kim J, Ryu B, Lee SG, Baek J, Kim YJ, Lee JM, Lee Y, Choi SO, Woo DH. Establishment of neurotoxicity assessment using microelectrode array (MEA) with hiPSC-derived neurons and evaluation of new psychoactive substances (NPS). Int J Stem Cells. 2022;15(3):258–69. https://doi.org/10.15283/ijsc21217.
15. Kirwan P, Turner-Bridger B, Peter M, Momoh A, Arambepola D, Robinson HPC, Livesey FJ. Development and function of human cerebral cortex

neural networks from pluripotent stem cells in vitro. Development. 2015;142(18):3178–87. https://doi.org/10.1242/DEV.123851/VIDEO-5.
16. Liu W, Han K, Sun M, Wang J. Enhancement and control of neuron adhesion on polydimethylsiloxane for cell microengineering using a functionalized triblock polymer. Lab Chip. 2019;19(19):3162–7. https://doi.org/10.1039/C9LC00736A.
17. Maccione A, Gandolfo M, Massobrio P, Novellino A, Martinoia S, Chiappalone M. A novel algorithm for precise identification of spikes in extracellularly recorded neuronal signals. J Neurosci Methods. 2009;177(1):241–9. https://doi.org/10.1016/J.JNEUMETH.2008.09.026.
18. Malenka RC, Nicoll RA. NMDA-receptor-dependent synaptic plasticity: multiple forms and mechanisms. Trends Neurosci. 1993;16(12):521–7. https://doi.org/10.1016/0166-2236(93)90197-T.
19. McCready FP, Gordillo-Sampedro S, Pradeepan K, Martinez-Trujillo J, Ellis J. Multielectrode arrays for functional phenotyping of neurons from induced pluripotent stem cell models of neurodevelopmental disorders. Biology. 2022;11(2):316. https://doi.org/10.3390/biology11020316.
20. Ming Y, Abedin MJ, Tatic-Lucic S, Berdichevsky Y. Microdevice for directional axodendritic connectivity between micro 3D neuronal cultures. Microsyst Nanoeng. 2021;7(1):1–13. https://doi.org/10.1038/s41378-021-00292-9.
21. Mossink B, Van Rhijn JR, Wang S, Linda K, Vitale MR, Zöller JE, van Hugte EJ, Bak J, Verboven AH, Selten M, Negwer M, Latour BL, van der Werf I, Keller JM, Klein TM, Gunnewiek CS, Oudakker A, Anania A, Jansen S, Lesch K-P, Frega M, van Bokhoven H, Schubert D, Kasri NN. Cadherin-13 is a critical regulator of GABAergic modulation in human stem-cell-derived neuronal networks. Mol Psychiatry. 2022;27(1):1–18. https://doi.org/10.1038/s41380-021-01117-x.
22. Mossink B, Verboven AHA, van Hugte EJH, Klein Gunnewiek TM, Parodi G, Linda K, Schoenmaker C, Kleefstra T, Kozicz T, van Bokhoven H, Schubert D, Nadif Kasri N, Frega M. Human neuronal networks on micro-electrode arrays are a highly robust tool to study disease-specific genotype-phenotype correlations in vitro. Stem Cell Rep. 2021;16(9):2182–96. https://doi.org/10.1016/j.stemcr.2021.07.001.
23. Nimtz L, Hartmann J, Tigges J, Masjosthusmann S, Schmuck M, Keßel E, Theiss S, Köhrer K, Petzsch P, Adjaye J, Wigmann C, Wieczorek D, Hildebrandt B, Bendt F, Hübenthal U, Brockerhoff G, Fritsche E. Characterization and application of electrically active neuronal networks established from human induced pluripotent stem cell-derived neural progenitor cells for neurotoxicity evaluation. Stem Cell Res. 2020;45:101761. https://doi.org/10.1016/j.scr.2020.101761.
24. Parodi G, Brofiga M, Pastore VP, Chiappalone M, Martinoia S. Deepening the role of excitation/inhibition balance in human iPSCs-derived neuronal networks coupled to MEAs during long-term development. J Neural Eng. 2023;20(5): 056011. https://doi.org/10.1088/1741-2552/ACF78B.
25. Pasquale V, Martinoia S, Chiappalone M. A self-adapting approach for the detection of bursts and network bursts in neuronal cultures. J Comput Neurosci. 2010;29(1–2):213–29. https://doi.org/10.1007/s10827-009-0175-1.
26. Pelkonen A, Pistono C, Klecki P, Gómez-Budia M, Dougalis A, Konttinen H, Stanová I, Fagerlund I, Leinonen V, Korhonen P, Malm T. Functional characterization of human pluripotent stem cell-derived models of the brain with microelectrode arrays. Cells. 2022;11(1):106. https://doi.org/10.3390/cells11010106.
27. Pinar N. Effects of tempol on epileptic activity in picrotoxin-induced epilepsy in rats. Neurol India. 2021;69(2):426–9. https://doi.org/10.4103/0028-3886.314542.
28. Sahara S, Yanagawa Y, O'Leary DDM, Stevens CF. The fraction of cortical GABAergic neurons is constant from near the start of cortical neurogenesis to adulthood. J Neurosci. 2012;32(14):4755–61. https://doi.org/10.1523/JNEUROSCI.6412-11.2012.
29. Salinas E, Sejnowski TJ. Correlated neuronal activity and the flow of neural information. Nat Rev Neurosci. 2001;2(8):539–50. https://doi.org/10.1038/35086012.
30. Shi Z, Zhang J, Chen S, Li Y, Lei X, Qiao H, Zhu Q, Hu B, Zhou Q, Jiao J. Conversion of fibroblasts to parvalbumin neurons by one transcription factor, Ascl1, and the chemical compound forskolin. J Biol Chem. 2016;291(26):13560–70. https://doi.org/10.1074/jbc.M115.709808.
31. Straub H, Köhling R, Speckmann EJ. Picrotoxin-induced epileptic activity in hippocampal and neocortical slices (guinea pig): suppression by organic calcium channel blockers. Brain Res. 1994;658(1–2):119–26. https://doi.org/10.1016/S0006-8993(09)90017-8.
32. Tang X, Zhou L, Wagner AM, Marchetto MCN, Muotri AR, Gage FH, Chen G. Astroglial cells regulate the developmental timeline of human neurons differentiated from induced pluripotent stem cells. Stem Cell Res. 2013;11(2):743–57. https://doi.org/10.1016/j.scr.2013.05.002.
33. Van De Vijver S, Missault S, Van Soom J, Van Der Veken P, Augustyns K, Joossens J, Dedeurwaerdere S, Giugliano M. The effect of pharmacological inhibition of serine proteases on neuronal networks in vitro. PeerJ. 2019;2019(4):e6796. https://doi.org/10.7717/PEERJ.6796/SUPP-1.
34. Wang S, Hesen R, Mossink B, Nadif Kasri N, Schubert D. Generation of glutamatergic/GABAergic neuronal co-cultures derived from human induced pluripotent stem cells for characterizing E/I balance in vitro. STAR Protocols. 2023;4(1):101967. https://doi.org/10.1016/j.xpro.2022.101967.
35. Woodruff G, Phillips N, Carromeu C, Guicherit O, White A, Johnson M, Zanella F, Anson B, Lovenberg T, Bonaventure P, Harrington AW. Screening for modulators of neural network activity in 3D human iPSC-derived cortical spheroids. PLoS ONE. 2020;15(10):e0240991. https://doi.org/10.1371/JOURNAL.PONE.0240991.
36. Ylä-Outinen L, Heikkilä J, Skottman H, Suuronen R, Äänismaa R, Narkilahti S. Human cell-based micro electrode array platform for studying neurotoxicity. Front Neuroeng. 2010;3:1–9. https://doi.org/10.3389/fneng.2010.00111.
37. Zhang Y, Pak CH, Han Y, Ahlenius H, Zhang Z, Chanda S, Marro S, Patzke C, Acuna C, Covy J, Xu W, Yang N, Danko T, Chen L, Wernig M, Südhof TC. Rapid single-step induction of functional neurons from human pluripotent stem cells. Neuron. 2013;78(5):785–98. https://doi.org/10.1016/j.neuron.2013.05.029.

Publisher's Note